Title	First-principles calculations of the ferroelastic transition between rutile-type and CaCl2-type SiO2 at high pressures
Author(s)	Togo, Atsushi; Oba, Fumiyasu; Tanaka, Isao
Citation	PHYSICAL REVIEW B (2008), 78(13)
Issue Date	2008-10
URL	http://hdl.handle.net/2433/84631
Right	© 2008 The American Physical Society
Type	Journal Article
Textversion	publisher

First-principles calculations of the ferroelastic transition between rutile-type and $CaCl_2$-type SiO_2 at high pressures

Atsushi Togo,[1,*] Fumiyasu Oba,[1] and Isao Tanaka[1,2]
[1]*Department of Materials Science and Engineering, Kyoto University, Sakyo, Kyoto 606-8501, Japan*
[2]*Nanostructures Research Laboratory, Japan Fine Ceramics Center, Atsuta, Nagoya 456-8587, Japan*
(Received 14 May 2008; revised manuscript received 19 September 2008; published 14 October 2008)

The tetragonal to orthorhombic ferroelastic phase transition between rutile- and $CaCl_2$-type SiO_2 at high pressures is studied using first-principles calculations and the Landau free-energy expansion. The phase transition is systematically investigated in terms of characteristic phonon modes with B_{1g} and A_g symmetries, shear moduli, transverse-acoustic mode, rotation angle of the SiO_6 octahedra, spontaneous symmetry-breaking and volume strains, and enthalpy. The results show that these physical behaviors at the transition are well described using the Landau free-energy expansion parametrized by the first-principles calculations.

DOI: 10.1103/PhysRevB.78.134106 PACS number(s): 62.50.−p, 62.20.de, 63.20.−e, 61.50.Ks

I. INTRODUCTION

Rutile-type SiO_2, which is called stishovite, transforms to $CaCl_2$-type SiO_2 upon applying high pressure. The tetragonal $(P4_2/mnm) \rightleftharpoons$ orthorhombic $(Pnnm)$ transition was found to be consistent with a classical second-order transition.[1] This transition is known as a prototypical pseudoproper ferroelastic transition, which is characterized by strain/order-parameter coupling. The transition is driven by B_{1g} mode softening. However, the strain/order-parameter coupling results in the transition having a nonzero soft-mode frequency.

The transition has been studied by experiments and first-principles calculations.[1–19] Before the orthorhombic phase was observed in experiments, the transition had been predicted on the basis of B_{1g} phonon-mode softening in the tetragonal phase. An observation of the orthorhombic phase was reported by Tsuchida and Yagi.[2] The transition pressure of about 45 GPa was predicted by Cohen using first-principles calculations.[3] He showed that the tetragonal shear modulus vanishes at the transition pressure and that the B_{1g} mode does not become unstable until the pressure reaches about 75 GPa. Kingma *et al.*[6] reported the transition pressure of 50 GPa using the Raman spectra of the B_{1g} mode in the tetragonal phase and the A_g mode in the orthorhombic phase. The transition pressure of 64 GPa was reported by Lee and Gonze[7] by a first-principles calculation of the tetragonal shear modulus. They showed that the acoustic mode is unstable at 73 GPa, which is lower than the pressure of 86 GPa at which the B_{1g} mode frequency vanishes.[8] Karki *et al.*[9–11] reported the transition pressure of about 47 GPa through investigations of the vanishing tetragonal shear modulus and the Raman-active modes using first-principles calculations. The similarity of the transition to a Landau-type temperature-induced transition was reported by Andrault *et al.*[1] using Rietveld structural analysis, which gave the transition pressure of 54 GPa.

Carpenter and *et al.*[12,13,19] employed the Landau free-energy expansion to explain the transition phenomena. They parametrized the Landau free-energy expansion using the experimental results. Although a number of studies based on first-principles calculations have been reported for this transition as mentioned above,[3,7,9,10,17,18] the results have not been connected to the Landau free-energy expansion. In this study, the ferroelastic transition of stishovite is investigated using first-principles calculations and the Landau free-energy expansion.

A unit cell of the tetragonal phase is shown in Fig. 1(a). It is made of two silicon and four oxygen atoms. A silicon atom and six surrounding oxygen atoms form SiO_6 tetrahedron. The octahedra on the same *a-b* plane share their apexes and the octahedra along the *c*-axis direction share their edges. From the viewpoint of the octahedral connection, the orthorhombic structure is equivalent to the tetragonal structure. The B_{1g} mode in the tetragonal phase and the A_g mode in the orthorhombic phase show characteristic behavior. These modes correspond to rotational vibrations of the octahedra

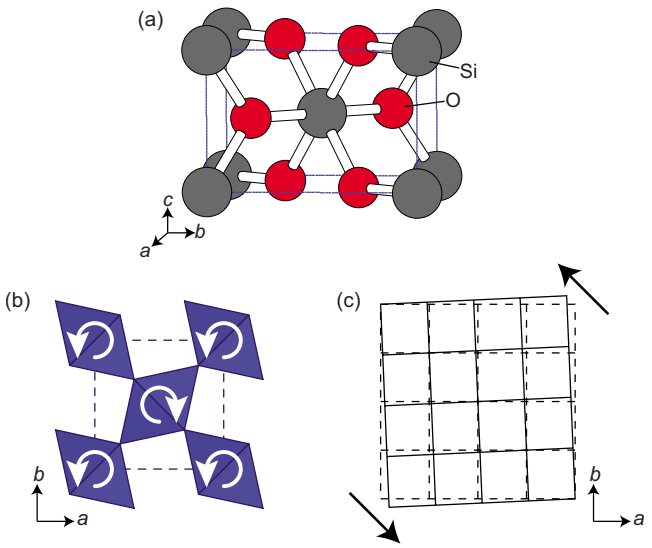

FIG. 1. (Color online) (a) Unit cell of the rutile-type structure. The dark gray and light gray (red) denote silicon and oxygen atoms, respectively. (b) Polyhedral representation of the B_{1g} (A_g) mode of the tetragonal (orthorhombic) structure projected onto the *a-b* plane. The directions of the octahedral rotations are depicted by arrows. The square with dashed lines represents the unit cell. (c) Schematic representation of the tetragonal shear strain. The dashed and solid lines represent the tetragonal and orthorhombic lattices, respectively. The arrows show the shear direction.

around the c axis as shown in Fig. 1(b). The directions of the rotations between adjacent octahedra are opposite. These modes involve only displacements of the oxygen atoms parallel to the a-b plane. Above the transition pressure, the octahedra at equilibrium start to rotate and symmetry-breaking spontaneous strain is generated. The shear strain corresponding to the tetragonal to orthorhombic lattice deformation is shown in Fig. 1(c)

II. LANDAU FREE-ENERGY EXPANSION

In this section, the Landau free-energy expansion of stishovite developed by Carpenter and *et al.*[12,19] is summarized following Ref. 12. Using the Landau free-energy expansion, excess energy G of the orthorhombic structure relative to the tetragonal structure is expanded by an order parameter and the components of strain, up to fourth and second orders, respectively,

$$\begin{aligned} G = {} & \frac{1}{2}a(P-P_c)Q^2 + \frac{1}{4}bQ^4 + \lambda_1(e_1+e_2)Q^2 + \lambda_2(e_1-e_2)Q \\ & + \lambda_3 e_3 Q^2 + \lambda_4(e_4^2-e_5^2) + \lambda_6 e_6^2 Q^2 + \frac{1}{4}(c_{11}^0+c_{12}^0)(e_1+e_2)^2 \\ & + \frac{1}{4}(c_{11}^0-c_{12}^0)(e_1-e_2)^2 + c_{13}^0(e_1+e_2)e_3 + \frac{1}{2}c_{33}^0 e_3^2 \\ & + \frac{1}{2}c_{44}^0(e_4^2+e_5^2) + \frac{1}{2}c_{66}^0 e_6^2, \end{aligned} \tag{1}$$

where a and b are the normal Landau coefficients, P is the applied pressure, P_c is the critical pressure, Q is the driving order parameter, e_1–e_6 are the components of spontaneous strain in Voigt notation, and λ_1–λ_6 are the strain/order-parameter coupling coefficients. c_{ij}^0 are the bare elastic stiffness constants which would be measured in the absence of a phase transition and change of equilibrium value of Q.[20] c_{ij}^0 and Q depend on pressure. The pressure dependences of a, b, and λ_i are expected to be weak, which will be discussed in Sec. IV. Though in fact pressure varies slightly with applying strain,[21] constant pressure is assumed when the applied strain is small as long as the second-order expansion by strain is valid.[22]

Equation (1) is rewritten as

$$G = \frac{1}{2}a(P-P_c^*)Q^2 + \frac{1}{4}b^*Q^4, \tag{2}$$

where P_c^* is the renormalized critical pressure corresponding to the transition pressure, and b^* is the renormalized fourth-order coefficient. The conditions of Q, e_1-e_2, e_1+e_2, and e_3 at equilibrium are written as

$$\frac{\partial G}{\partial Q}=0, \quad \frac{\partial G}{\partial(e_1-e_2)}=0, \quad \frac{\partial G}{\partial(e_1+e_2)}=0, \quad \frac{\partial G}{\partial e_3}=0. \tag{3}$$

e_4, e_5, and e_6 are zeros in the cases of tetragonal and orthorhombic symmetries. From these conditions, the phase-transition pressure P_c^* is obtained as

$$P_c^* = P_c + \frac{2\lambda_2^2}{a(c_{11}^0-c_{12}^0)}, \tag{4}$$

and b^* is given by

$$b^* = b - 2\frac{\lambda_3^2(c_{11}^0+c_{12}^0)+2\lambda_1^2 c_{33}^0 - 2\lambda_1\lambda_3(c_{13}^0+c_{33}^0)}{c_{33}^0(c_{11}^0+c_{12}^0)-2c_{13}^{0\,2}}. \tag{5}$$

The symmetry-breaking strain e_1-e_2, nonsymmetry-breaking strain e_1+e_2, and e_3 vary with Q as

$$e_1 - e_2 = -\frac{2\lambda_2}{c_{11}^0-c_{12}^0}Q, \tag{6}$$

$$e_1 + e_2 = \frac{2(\lambda_3 c_{13}^0 - \lambda_1 c_{33}^0)}{c_{33}^0(c_{11}^0+c_{12}^0)-2c_{13}^{0\,2}}Q^2, \tag{7}$$

$$e_3 = \frac{2\lambda_1 c_{13}^0 - \lambda_3(c_{11}^0+c_{12}^0)}{c_{33}^0(c_{11}^0+c_{12}^0)-2c_{13}^{0\,2}}Q^2. \tag{8}$$

The pressure dependence of the order parameter is given by

$$Q^2 = \begin{cases} 0, & P < P_c^*, \\ \dfrac{a}{b^*}(P_c^*-P), & P > P_c^*. \end{cases} \tag{9}$$

The second derivative of the excess energy G with respect to the order parameter under constant strain conditions at equilibrium is called the inverse order-parameter susceptibility χ^{-1}.[23,24] This is given by[12,19,20]

$$\begin{aligned} \chi^{-1} &= a(P-P_c) + 3bQ^2 \\ &= \begin{cases} a(P-P_c), & P < P_c^*, \\ a\left(3\dfrac{b}{b^*}-1\right)(P_c^*-P) + a(P_c^*-P_c), & P > P_c^*. \end{cases} \end{aligned} \tag{10}$$

Since the squared frequencies of the B_{1g} and A_g modes are expected to be proportional to χ^{-1},[25] they are also linearly dependent on pressure.

The elastic stiffness constants are given by[23]

$$c_{ij} = c_{ij}^0 - \chi\frac{\partial^2 G}{\partial e_i\,\partial Q}\frac{\partial^2 G}{\partial e_j\,\partial Q}. \tag{11}$$

Therefore, c_{11} and c_{12} in the tetragonal phase are

$$c_{11} = c_{11}^0 - \lambda_2^2\chi, \tag{12}$$

$$c_{12} = c_{12}^0 + \lambda_2^2\chi. \tag{13}$$

The shear modulus in the tetragonal phase $(c_{11}-c_{12})/2$ is obtained from Eqs. (4), (10), (12), and (13) as[12]

$$\frac{c_{11}-c_{12}}{2} = \frac{c_{11}^0-c_{12}^0}{2}\frac{P-P_c^*}{P-P_c}. \tag{14}$$

Similarly, c_{11}, c_{22}, and c_{12} in the orthorhombic phase are

$$c_{11} = c_{11}^0 - (4\lambda_1^2Q^2 + 4\lambda_1\lambda_2 Q + \lambda_2^2)\chi, \tag{15}$$

$$c_{22} = c_{22}^0 - (4\lambda_1^2 Q^2 - 4\lambda_1\lambda_2 Q + \lambda_2^2)\chi, \tag{16}$$

$$c_{12} = c_{12}^0 - 2(4\lambda_1^2 Q^2 - \lambda_2^2)\chi. \tag{17}$$

From Eqs. (4), (10), and (15)–(17), the shear modulus in the orthorhombic phase $(c_{11}+c_{22}-2c_{12})/4$ is given by

$$\frac{c_{11}+c_{22}-2c_{12}}{4} = \frac{c_{11}^0 - c_{12}^0}{2}\frac{P-P_c^*}{P-P_c^o}, \tag{18}$$

where P_c^o is the orthorhombic critical pressure, which is defined by

$$P_c^o = P_c^* + \frac{P_c^* - P_c}{3b/b^* - 1}. \tag{19}$$

The elastic stiffness constants are originally defined by[10]

$$c_{ij} = \Delta\sigma_i / e_j, \tag{20}$$

where $\Delta\sigma_i$ are the changes in the components of stress upon applying strain. We use the elastic stiffness constants to describe the formulae instead of the elastic constants used in Ref. 12, since the elastic stiffness constants are formally related to energy by[22,26]

$$c_{ij} = \frac{\partial^2 G}{\partial e_i \partial e_j}, \tag{21}$$

where G is assumed to be normalized by unit volume. In contrast, the elastic constants C_{ij} are defined by

$$C_{ij} = \frac{\partial^2 E}{\partial e_i \partial e_j}, \tag{22}$$

where E is the internal energy per unit volume. Therefore, c_{ij} are not equivalent to C_{ij} under pressure,[10,22] and thus the elastic stiffness constants are considered more suitable for use than the elastic constants.

III. METHOD OF CALCULATION

A. Phonon

Phonon calculations were performed using the Parlinski-Li-Kawazoe method[27] as implemented in the FROPHO code.[28] Phonon frequencies were obtained within harmonic approximation by solving the secular equations of dynamical matrices. Force-constant matrices Φ are written as[25,29]

$$\Phi_{\alpha\beta}\begin{pmatrix} jj' \\ ll' \end{pmatrix} = -\frac{F_\alpha(jl)}{\Delta u_\beta(j'l')}, \tag{23}$$

where subscripts α and β denote the Cartesian components, and jl and $j'l'$ denote the j and j'th atoms in the l and l'th unit cells, respectively. F_α is the α component of force on an atom and Δu_β is the β component of the atomic displacement from equilibrium position. This method of obtaining the force constants from forces and finite atomic displacements using supercells follows that developed by Parlinski *et al.*[27] and is explained in the FROPHO manual.[28] In this study, the forces were obtained using first-principles calculations.

The dynamical matrices **D** are written as

$$\mathbf{D}_{\alpha\beta}(jj',\mathbf{k}) = \frac{1}{(m_j m_{j'})^{1/2}}\sum_{l'}\Phi_{\alpha\beta}\begin{pmatrix} jj' \\ 0l' \end{pmatrix} \times \exp(i\mathbf{k}\cdot[\mathbf{r}(j'l') - \mathbf{r}(j0)]), \tag{24}$$

where m_j is the jth atomic mass, $\mathbf{r}(j'l')$ is the position of the j'th atom in the l'th unit cell, and $\mathbf{k}$ is the wave vector. Using the dynamical matrix, the secular equation is written as

$$\omega^2 \mathbf{e}(\mathbf{k},\nu) = \mathbf{D}(\mathbf{k})\cdot\mathbf{e}(\mathbf{k},\nu), \tag{25}$$

where ω and $\mathbf{e}(\mathbf{k},\nu)$ are the phonon frequency and eigenvector, respectively, and ν is the label of the solution.

B. Computational details

For the first-principles calculations, we employed the plane-wave basis projector augmented wave (PAW) method[30] in the framework of density-functional theory within the generalized gradient approximation in the Perdew-Burke-Ernzerhof form[31] as implemented in the VASP code.[32–34] A plane-wave energy cutoff of 500 eV was used. To avoid the discontinuity of calculated physical properties, we fixed the fast Fourier transform (FFT) mesh numbers of unit cells to those of the unit cell having the largest volume. The radial cutoffs of the PAW potentials of Si and O were 1.50 and 1.52 Å, respectively. The $3s$ and $3p$ electrons for Si and the $2s$ and $2p$ electrons for O were treated as valence and the remaining electrons were kept frozen. The Brillouin zones of the tetragonal and orthorhombic unit cells were sampled by $4\times4\times6$ k-point meshes generated in accordance with the Monkhorst-Pack scheme.[35] The total energy was minimized until the energy convergence became less than 1×10^{-6} eV. To obtain the equilibrium structures of unit cells at applied pressures, internal atomic positions were optimized until the residual forces became less than 1×10^{-3} eV/Å. Lattice parameters were optimized until the difference between each component of the specified and calculated stress became less than 1×10^{-2} GPa.

To obtain the force constants for the phonon calculations, atomic displacements of 0.01 Å were employed. Displacements in opposite directions along the a and b axes were incorporated in the calculations of force constants to improve the precision.

IV. RESULTS AND DISCUSSION

A. B_{1g} and A_g modes

The squared phonon frequencies of the B_{1g} and A_g modes calculated using the $2\times2\times3$ supercells as a function of pressure are shown in Fig. 2. As expected from Eq. (10), they are linearly dependent on pressure except at very low pressures. The calculated values of the B_{1g} mode between 10 and 100 GPa are fitted by a straight line $-538P+51743$ cm^{-2}. The values of the A_g mode between 54 and 120 GPa are fitted by $1308P-46696$ cm^{-2}. The transition pressure P_c^* is given by 53.3 GPa where these two lines intersect. This is considered to agree with the transition pressures of experiments 51.6,[6,12,13,19] 54,[1] and ~50 GPa.[13] The critical pressure P_c, which is determined from Eq. (10), is the pressure at

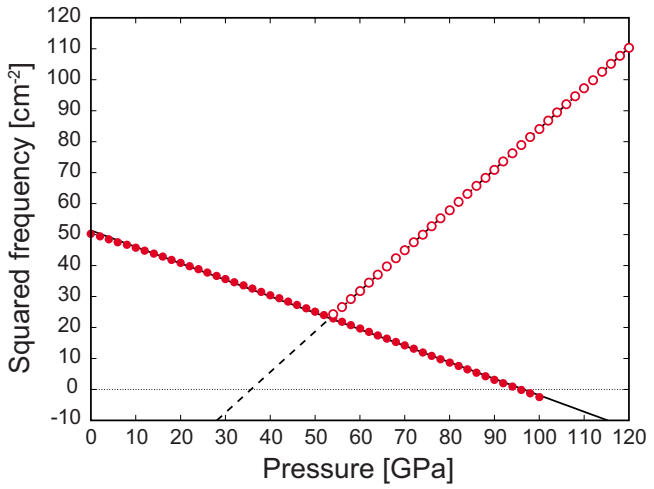

FIG. 2. (Color online) Squared frequencies of the B_{1g} and A_g modes as a function of pressure. The filled and open circles depict the values for the tetragonal and orthorhombic structures, respectively. The solid and dashed lines are the fits to respective values.

which the frequency of the B_{1g} mode vanishes and is given by the fit as 96.2 GPa. A Raman result gives $P_c = 102.3$ GPa.[6,12,13,19] The orthorhombic critical pressure P_c^o, which is determined from Eqs. (10) and (19), is the pressure at which the frequency of the A_g mode vanishes and is given by the fit as 35.7 GPa. The Raman result gives $P_c^o = 29.3$ GPa.[6,12,13,19] The calculated P_c and P_c^o are different from the experimental values by about 6 GPa. The ratio of the slopes of the squared frequencies was calculated as 2.43, which is greater than the experimental value of 2.27.[6,12,13,19]

The values of P_c^*, P_c, and P_c^o determined in this section are taken as reference values in Secs. IV B–IV F, since the use of B_{1g} and A_g modes is the most unambiguous method of determining these values among those discussed in this study.

B. Order parameter

The order parameter Q is considered to be proportional to the angle ϕ of the octahedral rotation, i.e., $Q \propto |\phi|$. The rotation angle is represented in the following two ways:[36]

$$\phi = \arctan\left[\frac{b_o(0.5-y)}{a_o(0.5-x)}\right] - 45, \tag{26}$$

and

$$\phi' = 45 - \arctan\left[\frac{b_o y}{a_o x}\right], \tag{27}$$

where ϕ and ϕ' are the rotation angles, a_o and b_o are the lattice parameters along the a and b axes, respectively, and x and y represent the internal atomic position of an oxygen atom on the face of the unit cell shown in Fig. 1(a) in the reduced coordinates. The difference between ϕ and ϕ' is obtained from the lengths of Si-O bonds projected onto the a-b plane. This difference between ϕ and ϕ' represents the torsion of the octahedron.

Under constant strain conditions with the tetragonal structure, Eq. (1) reduces to

$$G = \frac{1}{2}a(P-P_c)Q^2 + \frac{1}{4}bQ^4. \tag{28}$$

If the temperature effect is not considered, G is formally reduced to excess internal energy E, which is calculated as the internal energy relative to that at $\phi=0$ with the fixed lattice parameters. The values of E at various pressures were calculated as a function of the rotation angle ϕ. The rotations are given as atomic displacements along with the eigenvectors of the corresponding B_{1g} modes. As shown in Fig. 3(a), the energy required to rotate the octahedra decreases with increasing pressure. At 100 GPa, the structure at $\phi=0$ is no longer dynamically stable. However, the transition does not occur at the pressure at which the structure at $\phi=0$ becomes dynamically unstable but at the transition pressure P_c^*, since the transition pressure is renormalized by the strain/order-parameter coupling given by Eq. (4).

Since $Q \propto |\phi|$, E is represented by the following expansion using ϕ:

$$E(\phi) = A\phi^2 + B\phi^4 + O(\phi^6), \tag{29}$$

where A and B are the second- and fourth-order coefficients, respectively, which are proportional to $a(P-P_c)$ and b in Eq. (28), respectively. The odd-order terms disappear due to symmetry. A and B as a function of pressure, determined by fits to E, are shown in Fig. 3(b). As expected, A is linearly dependent on pressure and vanishes around the critical pressure obtained in Sec. IV A. B also depends linearly on pressure, hence the same holds for b.

Above the transition pressure, the octahedra at equilibrium start to rotate. The squared rotation angles ϕ and ϕ' as a function of pressure at equilibrium are shown in Fig. 3(c). The rotation angles increase with increasing pressure and nonlinearity is clearly observed. Since the torsion is smaller than that estimated from the lattice strain, it is considered that the rotation occurs to reduce the torsion of the octahedron.

Since the prefactors of pressure in Eq. (10) [a and $a(3b/b^*-1)$] are obtained as constants in Sec. IV A, the coefficient b^* is linearly dependent on pressure. Due to the pressure dependence of b^*, the squared order parameter Q^2 above the transition pressure in Eq. (9) is formally written as

$$\phi^2 \propto Q^2 = \alpha\frac{P-P_c^*}{P-\beta}, \tag{30}$$

where α and β are the constant parameters. This represents that the nonlinearity observed in Fig. 3(c) follows the pressure dependence of b^*. Using Eq. (30), the transition pressure is obtained by the fit as 53.4 GPa. This agrees well with that obtained in Sec. IV A (53.3 GPa).

C. Elasticity

As given by Eqs. (14) and (18), the shear moduli of the tetragonal and orthorhombic phases are related to a combination of the bare elastic stiffness constants $(c_{11}^0 - c_{12}^0)/2$. It is expected that the bare elastic stiffness constants can be calculated without relaxing the internal atomic positions. The pressure dependencies of $(c_{11}^0 - c_{12}^0)/2$ with strains of 0.001,

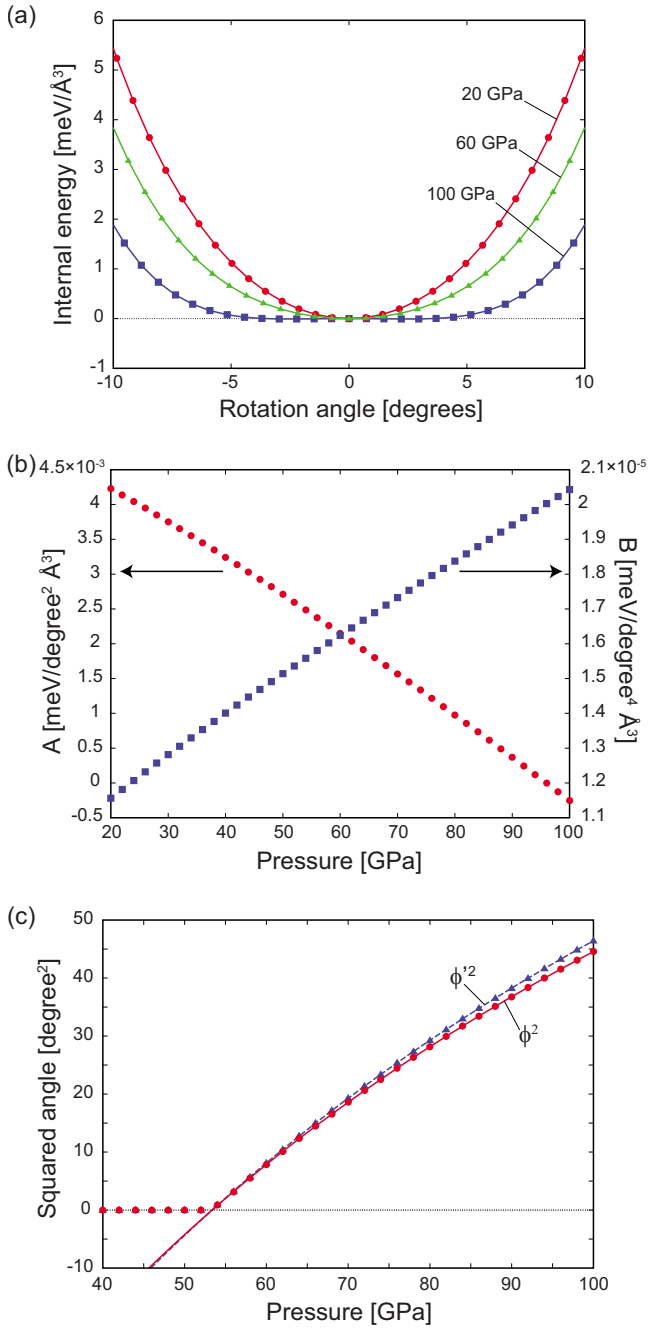

FIG. 3. (Color online) (a) Internal energies per unit volume as a function of the rotation angle ϕ relative to those at $\phi=0$. The circles, triangles, and squares denote the values at 20, 60, and 100 GPa, respectively. The curves through the symbols are guides for the eyes. (b) Second- and fourth-order coefficients A and B of Eq. (29) per unit volume as a function of pressure. The circles and squares denote A and B, respectively. (c) Squared rotation angles ϕ^2 and ϕ'^2 at equilibrium as a function of pressure. The circles and triangles depict ϕ and ϕ', respectively. The solid and dashed curves are the fits to ϕ and ϕ' above the transition pressure, respectively.

0.005, and 0.01 are shown in Fig. 4(a). The values are the averages of those calculated using positive and negative strains. They are approximately linearly dependent on pressure and the slope is positive. $(c_{11}^0-c_{12}^0)/2$ appears to be independent of the amount of strain.

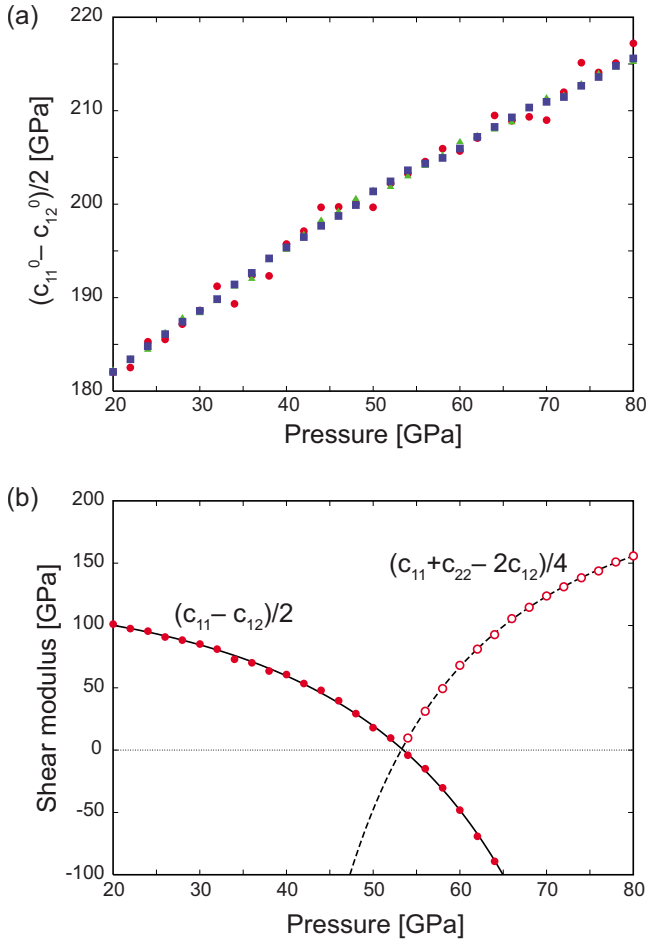

FIG. 4. (Color online) (a) $(c_{11}^0-c_{12}^0)/2$ as a function of pressure. The circles, squares, and triangles depict those calculated with strains of 0.001, 0.005, and 0.01, respectively. (b) $(c_{11}-c_{12})/2$ and $(c_{11}+c_{22}-2c_{12})/4$ as a function of pressure. Filled and open circles depict the values calculated using the tetragonal and orthorhombic structures, respectively, and the solid and dashed curves are the fits to the respective values.

Using Eq. (20), the elastic stiffness constants c_{ij} were obtained with a strain of 0.001. The strain e_1 reduces the tetragonal symmetry ($P4_2/mnm$) to the orthorhombic symmetry ($Pnnm$). Therefore, the internal atomic positions of all strained structures were relaxed under the constraints of $Pnnm$ symmetry. c_{12} of the orthorhombic structure was obtained by $c_{12}=(c_{12}+c_{21})/2$, since c_{12} is not equal to c_{21} under finite strain. The values obtained by positive and negative strains were averaged. The calculated shear moduli are shown in Fig. 4(b). The values for the tetragonal and orthorhombic structures were fitted using Eqs. (14) and (18), respectively, where $(c_{11}^0-c_{12}^0)/2$ is assumed to be linearly dependent on pressure. We obtained $P_c^*=53.5$ GPa and $P_c=97.1$ GPa by fitting to the values for the tetragonal structure and $P_c^*=53.2$ GPa and $P_c^o=28.4$ GPa by fitting to the values for the orthorhombic structure. These values of P_c^* agree well with that obtained in Sec. IV A (53.3 GPa). P_c and P_c^o are slightly different from the values obtained in Sec. IV A (102.3 and 29.3 GPa, respectively).

In fact, $(c_{11}^0-c_{12}^0)/2$ for the tetragonal and orthorhombic structures obtained by the fits are $1.10P+209$ and $-0.60P$

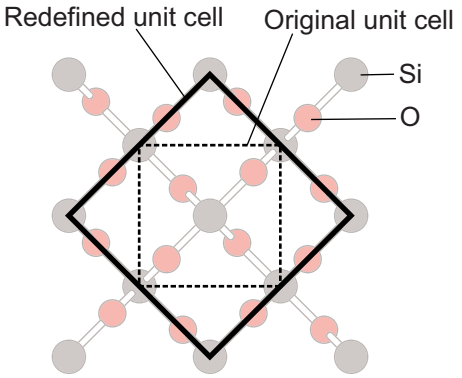

FIG. 5. (Color online) Redefined unit cell and original unit cell projected onto a-b plane, which are depicted by the solid and dashed lines, respectively. The number of atoms in the redefined unit cell is twice that in the original unit cell.

+348, respectively. These are inconsistent with the relation shown in Fig. 4(a).

D. Acoustic mode

The shear strain along the $[1\bar{1}0]$ direction corresponds to a transverse-acoustic (TA) mode with a wave vector along the [110] direction in the long-wavelength limit ($\mathbf{k}\rightarrow\mathbf{0}$). Since the group velocity in the long-wavelength limit is proportional to the shear modulus,[25] the group velocity of the TA mode at $\mathbf{k}\rightarrow\mathbf{0}$ vanishes at the transition pressure as well as the shear moduli.

The group velocity v_g is defined by

$$v_g(k) = \frac{\partial \omega_{\mathrm{TA}}(k)}{\partial k}, \tag{31}$$

where ω_{TA} is the phonon frequency of the TA mode. For a small $|\mathbf{k}|$, the group velocity at $\mathbf{k}\rightarrow\mathbf{0}$ is approximated by $\omega_{\mathrm{TA}}(\mathbf{k})/|\mathbf{k}|$. To obtain the phonon frequency for small $|\mathbf{k}|$, we employed a supercell elongated in the [110] direction by an $8\times1\times1$ expansion of the redefined unit cell that is shown in Fig. 5. The redefined unit cell is formed by rotating the original unit cell by 45°. The lattice vectors in the a-b plane are redefined along the [110] and $[1\bar{1}0]$ directions of the original unit cell.

TA-mode phonon branches between the Γ and M points calculated using the elongated supercell and the $2\times2\times3$ supercell at 20, 40, 60, and 80 GPa are shown in Fig. 6(a). The branches at 20 and 40 GPa were calculated using the tetragonal structures and those at 60 and 80 GPa were calculated using the orthorhombic structures. The circles on the solid curves are the k points whose atomic displacements fulfill the boundary condition of the elongated supercells. Therefore, the frequencies are expected to be correct within the approximations used in this study. When the atomic interaction range is sufficiently small compared with the supercell size, reasonable frequencies are obtained even if the k point is not represented exactly by the supercell. Indeed, the phonon branches of the $2\times2\times3$ supercells at 20 and 80 GPa are analogous to those of the elongated supercells.

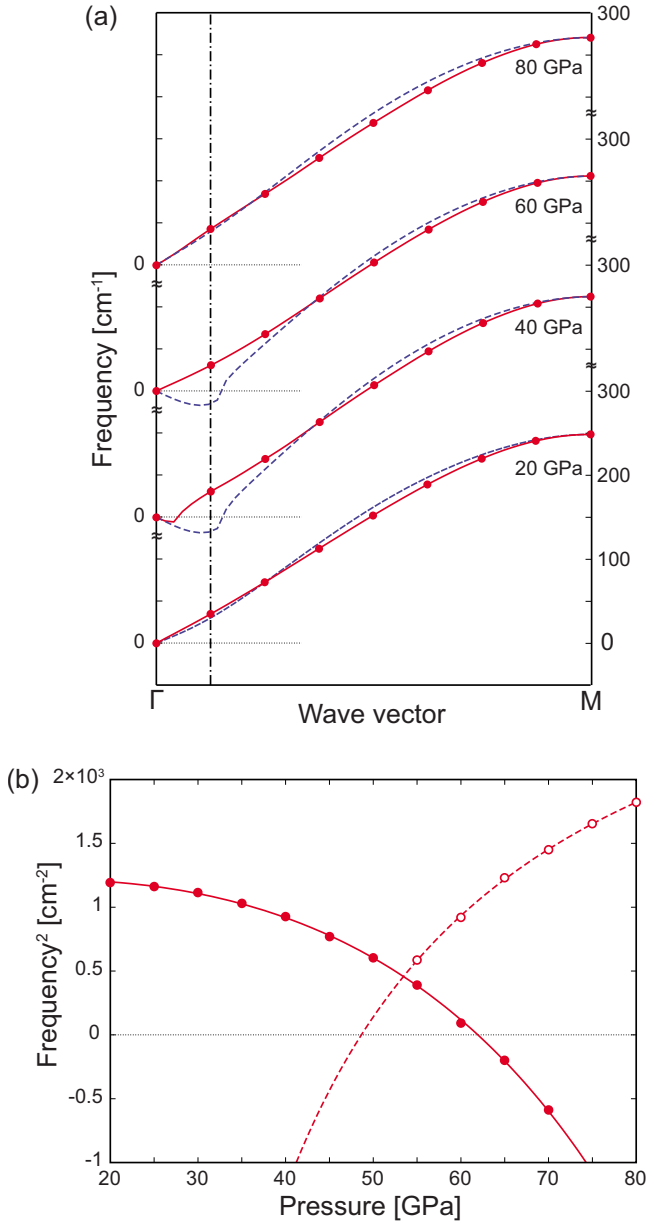

FIG. 6. (Color online) (a) TA-mode phonon branches using the elongated supercells (solid curves) and the $2\times2\times3$ supercells (dashed curves). The circles on the solid curves represent the exact k points represented by the elongated supercells. The vertical dashed-dotted line depicts $\mathbf{k}=[1/16,1/16,0]$. Imaginary frequencies are represented as negative values. (b) Squared TA-mode frequencies of the elongated supercell at $\mathbf{k}=[1/16,1/16,0]$ as a function of pressure. The filled and open circles show the values for the tetragonal and orthorhombic structures, respectively, and the solid and dashed curves are the fits to the respective values.

However, at 40 and 60 GPa, the branches of the $2\times2\times3$ supercells are markedly distorted near the Γ point. Even in the elongated supercells, an unexpected imaginary frequency appears at 40 GPa. This indicates that the atomic interaction range becomes larger than the supercell size as the pressure approaches the transition pressure.

The squared TA-mode frequencies calculated using the elongated supercell at $\mathbf{k}=[1/16,1/16,0]$ as a function of

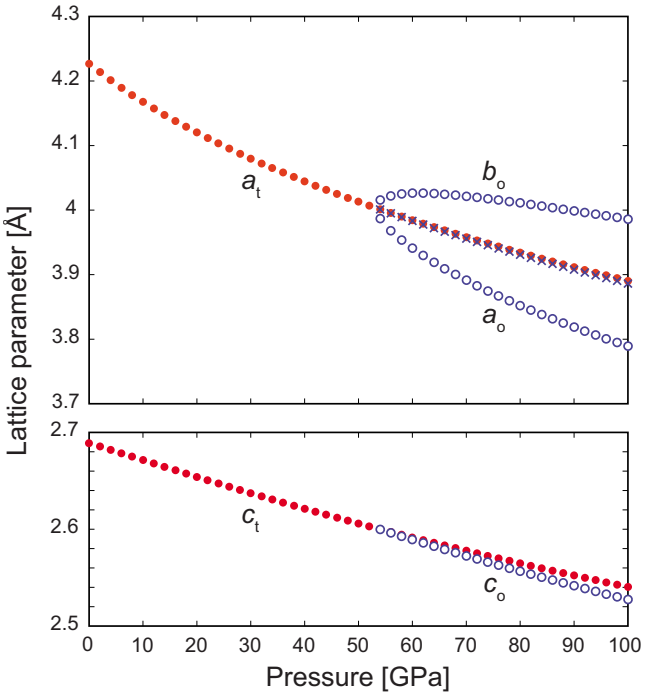

FIG. 7. (Color online) Lattice parameters as a function of pressure. The filled and open circles depict those of the tetragonal and orthorhombic structures, respectively. The crosses denote $\sqrt{a_o \times b_o}$.

pressure are shown in Fig. 6(b). $\mathbf{k}=[1/16,1/16,0]$ is the exact k point closest to the Γ point, and the position on the $\Gamma-\mathrm{M}$ path is depicted in Fig. 6(a). The squared frequencies for the tetragonal and orthorhombic structures were fitted by Eqs. (14) and (18) multiplied by proportionality coefficients, respectively. The corresponding values of P_c^* are incorrectly determined by the fits, although the values are fitted smoothly. This indicates that the elongated supercell is not sufficiently large to approximate the group velocity near the transition pressure. Nevertheless, the transition pressure is obtained as the pressure at which the curves intersect since the tetragonal and orthorhombic structures coincide at the transition pressure. The resultant value of 53.4 GPa agrees well with that obtained in Sec. IV A (53.3 GPa).

E. Strain

The strains e_1, e_2, and e_3 are defined as

$$e_1 = \frac{a_o - a_t}{a_t}, \quad e_2 = \frac{b_o - a_t}{a_t}, \quad e_3 = \frac{c_o - c_t}{c_t}, \tag{32}$$

where a_o, b_o, and c_o are the lattice parameters of the orthorhombic structure and a_t and c_t are those of the tetragonal structure. The lattice parameters as a function of pressure are shown in Fig. 7. a_t and c_t were calculated under the constraints of $P4_2/mnm$ symmetry even above the transition pressure. Since c_o and $\sqrt{a_o \times b_o}$ are smaller than a_t and c_t, respectively, the volume of the orthorhombic structure is smaller than that of the rutile structure.

The spontaneous symmetry-breaking strain e_1-e_2 appears above the transition pressure. From Eqs. (4), (6), and (9), the

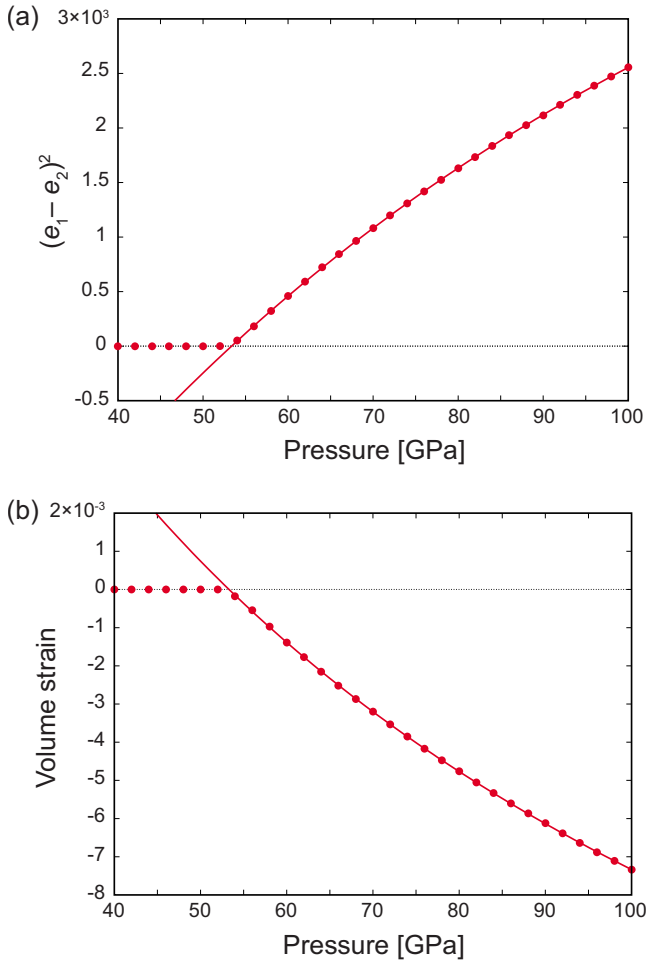

FIG. 8. (Color online) (a) Squared symmetry-breaking strain $(e_1-e_2)^2$ as a function of pressure. (b) Volume strain as a function of pressure. The curves are the fits to the values above the transition pressure.

squared symmetry-breaking strain is given by

$$(e_1 - e_2)^2 = \frac{2a^2(P_c^* - P_c)(P_c^* - P)}{b^*(c_{11}^0 - c_{12}^0)}. \tag{33}$$

The squared symmetry-breaking strain as a function of pressure is shown in Fig. 8(a). If we assume that b^* and $c_{11}^0 - c_{12}^0$ are linearly dependent on pressure, as discussed in Secs. IV B and IV C, the values are fitted well by Eq. (33). As a result, the transition pressure is given as 53.4 GPa, which agrees well with that obtained in Sec. IV A (53.3 GPa).

Volume strain V_s is defined as

$$V_s = \frac{V_o - V_t}{V_t}, \tag{34}$$

where V_t and V_o are the volumes of the tetragonal and orthorhombic structures, respectively. The volume strain calculated using the lattice parameters as a function of pressure is shown in Fig. 8(b). Since the volume strain is approximated by $e_1+e_2+e_3$, from Eqs. (7) and (8), it is given by

$$V_s = \frac{2\lambda_1(c_{13}^0 - c_{33}^0) + \lambda_3(2c_{13}^0 - c_{11}^0 - c_{12}^0)}{c_{33}^0(c_{11}^0 + c_{12}^0) - 2c_{13}^{0\,2}} Q^2. \quad (35)$$

If we assume that the prefactor of Q^2 is constant, the transition pressure is obtained as 53.3 GPa from the fit using Eq. (30). This agrees well with that obtained in Sec. IV A (53.3 GPa).

F. Enthalpy

Substituting Eq. (9) into Eq. (2), the excess energy G at equilibrium is given by

$$G = -\frac{1}{4}\frac{a^2}{b^*}(P - P_c^*)^2. \quad (36)$$

The excess energy G at 0 K is formally calculated by the excess enthalpy of the orthorhombic structure relative to that of the tetragonal structure. The excess enthalpy as a function of pressure normalized by the unit volume of the tetragonal structure is shown in Fig. 9. The values above 54 GPa are fitted by Eq. (36), where b^* is assumed to be linearly dependent on pressure. The transition pressure is obtained as 55.7 GPa by the fit, which is overestimated by ~2 GPa compared with that obtained in Sec. IV A (53.3 GPa). Employing enthalpy to determine the transition pressure is considered to be the most difficult method among those presented in this study.

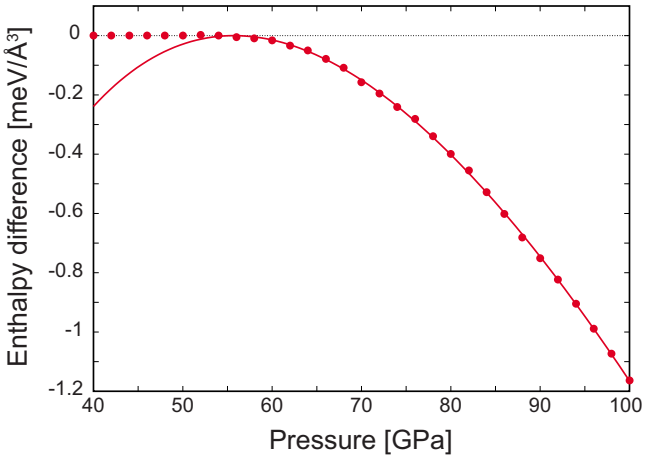

FIG. 9. (Color online) Enthalpy of the orthorhombic structure relative to that of the tetragonal structure as a function of pressure normalized by the unit volume of the tetragonal structure. The curve depicts the fit to the values above 54 GPa.

V. CONCLUSIONS

We studied the pseudoproper ferroelastic phase transition of stishovite using first-principles calculations in conjunction with the Landau free-energy expansion. Various phenomena related to the transition, the characteristic behaviors of the B_{1g} and A_g phonon modes, the vanishing shear moduli, the rotation of the octahedra, the spontaneous symmetry-breaking strain and volume strain, and the excess enthalpy were systematically investigated. The physical values predicted by the first-principles calculations are well described by the Landau free-energy expansion. In some cases, the pressure-dependent parameters of the Landau free-energy expansion are required to describe the nonlinear behaviors, as pointed out in Sec. VII of Ref. 12. The present results indicate that the combination of the first-principles calculation and the Landau free-energy expansion is useful for explaining and understanding the physical phenomena of the ferroelastic phase transition.

ACKNOWLEDGMENTS

This work was supported by three programs from the Ministry of Education, Culture, Sports, Science and Technology of Japan: the Grants-in-Aid for Scientific Research (A), Priority Area on "atomic scale modification" (No. 474), and the global COE program.

*togo.atsushi@gmail.com

[1] D. Andrault, G. Fiquet, F. Guyot, and M. Hanfland, Science **282**, 720 (1998).
[2] Y. Tsuchida and T. Yagi, Nature (London) **340**, 217 (1989).
[3] R. E. Cohen, in *High-Pressure Research: Application to Earth and Planetary Sciences*, Geophysical Monograph Series Vol. 67, edited by Y. Syono and M. H. Manghnani (American Geophysical Union, Washington, D.C., 1992), pp. 425–431.
[4] Y. Yamada, S. Tsuneyuki, and Y. Matsui, in *High-Pressure Research: Application to Earth and Planetary Sciences*, Geophysical Monograph Series Vol. 67, edited by Y. Syono and M. H. Manghnani (American Geophysical Union, Washington, D.C., 1992), pp. 441–446.
[5] R. J. Hemley, C. T. Prewitt, and K. J. Kingma, *Silica: Physical Behavior, Geochemistry and Materials Applications* (Mineralogical Society of America, Chantilly, 1994), Vol. 29, pp. 41–81.
[6] K. J. Kingma, R. E. Cohen, R. J. Hemley, and H. K. Mao, Nature (London) **374**, 243 (1995).
[7] C. Lee and X. Gonze, Phys. Rev. B **56**, 7321 (1997).
[8] C. Lee and X. Gonze, J. Phys.: Condens. Matter **7**, 3693 (1995).
[9] B. B. Karki, M. C. Warren, L. Stixrude, G. J. Ackland, and J. Crain, Phys. Rev. B **55**, 3465 (1997).
[10] B. B. Karki, G. J. Ackland, and J. Crain, J. Phys.: Condens. Matter **9**, 8579 (1997).
[11] B. B. Karki, L. Stixrude, and J. Crain, Geophys. Res. Lett. **24**, 3269 (1997).
[12] M. A. Carpenter, R. J. Hemley, and H. K. Mao, J. Geophys. Res. **105**, 10807 (2000).
[13] R. J. Hemley, J. Shu, M. A. Carpenter, J. Hu, H. K. Mao, and K. J. Kingma, Solid State Commun. **114**, 527 (2000).
[14] S. R. Shieh, T. S. Duffy, and B. S. Li, Phys. Rev. Lett. **89**, 255507 (2002).
[15] S. Ono, K. Hirose, M. Murakami, and M. Isshiki, Earth Planet. Sci. Lett. **197**, 187 (2002).

[16] M. Murakami, K. Hirose, S. Ono, and Y. Ohishi, Geophys. Res. Lett. **30**, 1207 (2003).
[17] T. Tsuchiya, R. Caracas, and J. Tsuchiya, Geophys. Res. Lett. **31**, L11610 (2004).
[18] A. R. Oganov, M. J. Gillan, and G. D. Price, Phys. Rev. B **71**, 064104 (2005).
[19] M. Carpenter, Am. Mineral. **91**, 229 (2006).
[20] M. A. Carpenter and E. K. H. Salje, Eur. J. Mineral. **10**, 693 (1998).
[21] G. Steinle-Neumann and R. E. Cohen, J. Phys.: Condens. Matter **16**, 8783 (2004).
[22] J. Wang, J. Li, S. Yip, S. Phillpot, and D. Wolf, Phys. Rev. B **52**, 12627 (1995).
[23] J. C. Slonczewski and H. Thomas, Phys. Rev. B **1**, 3599 (1970).
[24] E. K. H. Salje, *Phase Transitions in Ferroelastic and Co-Elastic Crystals* (Cambridge University Press, Cambridge, 1990).
[25] M. T. Dove, *Introduction to Lattice Dynamics* (Cambridge University Press, Cambridge, 1993).
[26] G. V. Sin'ko and N. A. Smirnov, J. Phys.: Condens. Matter **16**, 8101 (2004).
[27] K. Parlinski, Z. Q. Li, and Y. Kawazoe, Phys. Rev. Lett. **78**, 4063 (1997).
[28] A. Togo, FROPHO, http://fropho.sourceforge.net/
[29] R. M. Martin, *Electronic Structure* (Cambridge University Press, Cambridge, 2004).
[30] P. E. Blöchl, Phys. Rev. B **50**, 17953 (1994).
[31] J. P. Perdew, K. Burke, and M. Ernzerhof, Phys. Rev. Lett. **77**, 3865 (1996).
[32] G. Kresse, J. Non-Cryst. Solids **192-193**, 222 (1995).
[33] G. Kresse and J. Furthmüller, Comput. Mater. Sci. **6**, 15 (1996).
[34] G. Kresse and D. Joubert, Phys. Rev. B **59**, 1758 (1999).
[35] H. J. Monkhorst and J. D. Pack, Phys. Rev. B **13**, 5188 (1976).
[36] J. Haines, J. M. Leger, C. Chateau, and A. S. Pereira, Phys. Chem. Miner. **27**, 575 (2000).